Original paper

Biomechan Model Mechanobiol 1 (2003) 279 – 293 © Springer-Verlag 2003
DOI 10.1007/s10237-002-0020-1

Relationship between structural modeling and hyperelastic material behavior: application to CNS white matter

D. F. Meaney

Abstract Recent measurements of the material properties of brain tissue allow an examination of the underlying microstructural basis in both physiological and pathophysiological conditions. The purpose of this study is to develop a mathematical relationship between microstructurally based models of the central nervous system (CNS) white matter and equivalent hyperelastic material models. For simplicity, time dependent material behavior is not included in this formulation. The microstructural representation is used to formulate structural property relationships for highly oriented white matter, and is mathematically compared to one isotropic and two anisotropic hyperelastic formulations. For the anisotropic characterizations, the population of axons in the white matter is assumed to align along one preferred direction of the material, yielding a transversely isotropic formulation. Relatively simple strain–energy functions incorporating material anisotropy provide sufficient flexibility to model the nonlinear behavior predicted from structurally based models, although the tangential stiffness of the hyperelastic approaches does not follow completely the behavior of the structurally based formulations. This analysis is an initial step towards linking microstructural aspects of the tissue to material models commonly used for large deformations, and may be an important step in relating predicted tissue deformation to the deformation and stress of cellular and subcellular structures.

1
Introduction

Most poor neurologic outcomes in survivors of brain or spinal cord injury result from damage to the axonal process of neurons. Mild axonal damage appears as only a faint swelling of the axonal process, while severe axonal damage appears as a physical tear of the axonal process. Despite its significance, the in vivo mechanical parameters responsible for the traumatic white matter damage have been established only recently (Bain and Meaney 2000). It is not yet known, however, how macroscopic deformations and stresses that occur at the mechanical threshold levels are transferred to the underlying cellular structures of the white matter to cause injury.

Recent in vitro models demonstrate the importance of particular injury mechanisms for axonal damage and allow a better comparison of cellular deformation and response. These models do not contain the organotypic architecture present within the brain, however, and some axons only remain viable for hours following injury. Stretch studies on the myelinated fiber (Gray and Ritchie 1954; Saatman and Thibault 1993; Rydevik et al. 1990; Wall et al. 1991) indicate changes in fiber morphology, action potential propagation, and failure thresholds as the amount and rate of elongation are changed. These fiber preparations, though, are from peripheral nerve bundles and are difficult to maintain. Dynamically stretching an unmyelinated squid giant axon (Galbraith et al. 1993) causes a change in the resting membrane potential, and can elicit action potentials along the axon if the stretch is sufficiently large. Although important for mechanism studies, it is difficult to evaluate treatments

Received: 15 October 2001 / Accepted: 30 September 2002

D. F. Meaney
Department of Bioengineering,
3320 Smith Walk, University of Pennsylvania,
Philadelphia, PA 19104-6392, USA
E-mail: dmeaney@seas.upenn.edu
Tel.: +1-215-5733155
Fax: +1-215-5732071

Funds for this work were provided by CDC grant R49/CCR312712 and NIH grants P50 NS08803, NICHD RO1 41699, and NINDS RO1 35712.

in this model since even an uninjured axon survives for only a few hours in the saline bath. New cell culture models of axonal injury (for a review, see Morrison et al., 1998) offer promise in understanding more basic mechanisms of cell injury, but presently do not contain myelinated axons, mixed cell populations, or offer good measures of functional outcome.

A new in vivo model using the guinea pig optic nerve offers many advantages because it has the organotypic nature of in vivo central nervous system (CNS) tissue, can be quantifiably deformed in vivo, and reproduces the morphology of traumatic axonal damage in humans (Gennarelli et al. 1989). The nerve contains axonal processes from the retinal ganglion cells, astrocytes, oligodendrocytes, a vascular network, and is surrounded by a pia/arachnoid/dura sheath. A recent study using this model established the mechanical parameters associated with the onset of axonal injury in the optic nerve after a single, dynamic elongation (Bain and Meaney 2000). In this paper, structurally based material models of the optic nerve are developed that relate tissue strain to the deformation and stress of subcellular elements that occur during simple elongation of the optic nerve. It is envisioned that a continuum approximation to a structurally based model of white matter behavior will allow one to use computationally inexpensive material formulations to predict the response of the brain to impact, yet maintain a link to the microstructural aspects of the tissue and enable future predictions on the biological response of the cellular structures from impact or other forms of mechanical loading.

2
Development of the models

Of the many different approaches available for modeling soft tissue behavior, two approaches were used for this study: (a) an energy based hyperelastic approach to model the continuum properties, with a specific extension for modeling material anisotropy, and (b) a structural model approach to model the deformation of cellular structures within the material. Both approaches were used for modeling white matter tissue, since each has distinct advantages. Some common hyperelastic models are readily available in commercial finite element packages and therefore offer a means to rapidly use measured material properties in finite element simulations of the brain subjected to impact. Moreover, material anisotropy is readily incorporated into these models to model the anisotropic properties of brain tissue (Prange and Margulies 2002). In contrast, structural models are particularly useful to estimate thresholds for axons within the optic nerve, since these models are used to predict how individual axons within the optic nerve elongate during the in vivo tests. Moreover, these structural models will allow us to examine the thresholds in different regions of the brain by accounting for the geometric differences between two separate anatomic regions.

For simplicity, each model is formulated without time dependent material behavior. Future studies will incorporate viscoelastic behavior to improve the fidelity of each material model.

2.1
Hyperelastic formulations

For finite deformations, we consider a general state of deformation described by the deformation gradient tensor (**F**):

$$\mathbf{F}_{iR} = \frac{\partial x_i}{\partial X_R}, \quad i,R = 1, \ldots, 3 \ . \tag{1}$$

From this deformation gradient tensor, we define the right (**C**) and the left Cauchy-Green tensor (**B**). Thus,

$$\mathbf{C} = \mathbf{F}^T \cdot \mathbf{F} \ , \tag{2}$$

and,

$$\mathbf{B} = \mathbf{F} \cdot \mathbf{F}^T \ , \tag{3}$$

which have the following specific components:

$$C_{RS} = \frac{\partial x_i}{\partial X_R}\frac{\partial x_i}{\partial X_S} = F_{iR}F_{iS} \ , \tag{4}$$

and,

$$B_{ij} = \frac{\partial x_i}{\partial X_R}\frac{\partial x_j}{\partial X_R} = F_{iR}F_{jR} \ . \tag{5}$$

To incorporate material anisotropy, the approach used in this paper considers reinforcing fibers that are oriented along a specific direction in the undeformed state of the material (Spencer 1984). If the orientation of the fiber population is described by a unit vector ($\mathbf{a}_o$), it can be shown that the fiber stretch (λ_{fiber}) as a result of the applied deformation is:

$$\lambda^2_{\text{fiber}} = \frac{\partial x_i}{\partial X_R}\frac{\partial x_i}{\partial X_S} a_{o_R} a_{o_S} = C_{RS} a_{o_R} a_{o_S} = \mathbf{a}_o \cdot \mathbf{C} \cdot \mathbf{a}_o \ . \tag{6}$$

The strain–energy function is unchanged with a rigid body rotation of the reference state; as such, the strain–energy can be described as a function of the invariants:

$$I_1 = \text{tr}\mathbf{C} \ , \tag{7}$$

$$I_2 = \frac{1}{2}\left((\text{tr}\mathbf{C})^2 - \text{tr}\mathbf{C}^2\right) \ , \tag{8}$$

$$I_3 = \det\mathbf{C} \ , \tag{9}$$

$$I_4 = \mathbf{a}_o \cdot \mathbf{C} \cdot \mathbf{a}_o \ , \tag{10}$$

and,

$$I_5 = \mathbf{a}_o \cdot \mathbf{C}^2 \cdot \mathbf{a}_o \ . \tag{11}$$

One approach for developing a strain–energy function, W say, to describe an anisotropic material is splitting the function into distinct parts:

$$W = W(I_1, I_2) + W(I_4) + W(I_5) \ , \tag{12}$$

where the first component ($W(I_1,I_2)$) describes the isotropic response of the material, and the remaining two terms describe the directional properties introduced by the reinforcing fibers. An alternative approach is to express the isotropic response in terms of the principal stretches ($\lambda_1, \lambda_2, \lambda_3$), and describe the directional behavior separately through the fourth and fifth invariants:

$$W = W(\lambda_1, \lambda_2, \lambda_3) + W(I_4) + W(I_5) \ . \tag{13}$$

For a strain–energy function expressed only in terms of the five invariants, it has been shown (Spencer 1984) that the Cauchy stress tensor ($\boldsymbol{\sigma}$) for an incompressible material is expressed as:

$$\boldsymbol{\sigma} = 2\left\{\frac{\partial W}{\partial I_1}\mathbf{B} - \frac{\partial W}{\partial I_2}\mathbf{B}^{-1} + I_4\frac{\partial W}{\partial I_4}\mathbf{a}\otimes\mathbf{a} + I_4\frac{\partial W}{\partial I_5}(\mathbf{a}\otimes\mathbf{B}\cdot\mathbf{a} + \mathbf{a}\cdot\mathbf{B}\otimes\mathbf{a})\right\} - p\mathbf{I} \tag{14}$$

and p is a reaction pressure due to the material incompressibility. If the alternative approach (Eq. 13) is used, the stress tensor assumes a slightly different form:

$$\boldsymbol{\sigma} = \boldsymbol{\sigma}_{\text{isotropic}} + 2\left\{I_4\frac{\partial W}{\partial I_4}\mathbf{a}\otimes\mathbf{a} + I_4\frac{\partial W}{\partial I_5}(\mathbf{a}\otimes\mathbf{B}\cdot\mathbf{a} + \mathbf{a}\cdot\mathbf{B}\otimes\mathbf{a})\right\} - p\mathbf{I} \ , \tag{15}$$

where

$$\sigma_{ij,\text{isotropic}} = 2F_{iR}F_{jS}\sum_{a=1}^{3}\frac{\partial W}{\partial\lambda_a}\frac{\partial\lambda_a}{\partial C_{RS}} \ , \tag{16}$$

and $\boldsymbol{a} = \boldsymbol{F}\cdot\boldsymbol{a_0}$ denotes the fiber direction in the deformed configuration.

From the Cauchy stress description, the first Piola-Kirchhoff stress tensor ($\mathbf{T}$) can be computed directly:

$$T_{ij} = \sigma_{ia}\frac{\partial X_j}{\partial x_a} \ . \tag{17}$$

Simple tension gives ($\lambda_1 = \lambda, \quad \lambda_2 = \lambda_3 = \lambda^{-1/2}$)

$$[\mathbf{F}] = \begin{bmatrix} \lambda & 0 & 0 \\ 0 & 1/\sqrt{\lambda} & 0 \\ 0 & 0 & 1/\sqrt{\lambda} \end{bmatrix} , \tag{18}$$

where the material is considered incompressible. The axons represent the reinforcing "fibers" in an anisotropic formulation, are elongated along the axis of stretch, and, therefore, have the preferred direction:

$$\mathbf{a} = \mathbf{a}_o = x_1 + 0 \cdot x_2 + 0 \cdot x_3 = [1 \quad 0 \quad 0] . \tag{19}$$

Under simple extension along the x_1 axis, there are no shear forces ($T_{12} = T_{23} = T_{13} = 0$) and the surfaces normal to the x_2 and x_3 axis are traction free ($T_{22} = T_{33} = 0$).

In this analysis, three hyperelastic formulations are examined:

1. The Mooney–Rivlin formulation with no material anisotropy:

$$W(I_1, I_2) = \frac{\mu_1}{2}(I_1 - 3) + \frac{\mu_2}{2}(I_2 - 3) , \tag{20}$$

yielding,

$$T_{11} = \mu_1\left(\lambda - \frac{1}{\lambda^2}\right) - \mu_2\left(\frac{1}{\lambda^3} - 1\right) . \tag{21}$$

For this formulation, three ratios of μ_1/μ_2 will be used to reflect the range that has been used in other studies of CNS tissue ($\mu_1/\mu_2 = 0.10$, $\mu_1/\mu_2 = 1.0$, $\mu_1/\mu_2 = 10.0$ (Mendis et al. 1995)).

2. A simple anisotropic formulation described by Fung for soft tissues (Fung 1981):

$$W(I_1, I_4) = C\left(\exp(C_1(I_1 - 3) + C_2(I_4 - 1)^2) - 1\right) , \tag{22}$$

which yields the following stress along the x_1-axis:

$$T_{11} = 2C\exp(C_1(I_1 - 3) + C_2(I_4 - 1)^2)\left(C_1\left(\lambda - \frac{1}{\lambda^2}\right) + 2C_2\lambda\left(\lambda^2 - 1\right)\right) . \tag{23}$$

In this description, the ratio of C_2/C_1 is set to emphasize the stiffness of the axons relative to the surrounding isotropic matrix ($C_2/C_1 = 10.0$).

3. A first order Ogden description (Ogden 1984) for both the isotropic glial matrix (g) and the reinforcing axonal fiber network (a):

$$W = \frac{2\mu_g}{\alpha_g^2}\left(\lambda^{\alpha_g} + 2\lambda^{-\alpha_g/2} - 3\right) + \frac{2\mu_a}{\alpha_a^2}\left(I_4^{\alpha_a/2} + 2I_4^{-\alpha_a/4} - 3\right) , \tag{24}$$

where μ_i and α_i are material parameters. The strain–energy function in Eq. (24) yields the following first Piola–Kirchhoff stress (engineering stress) in the direction of the axonal fibers:

$$T_{11} = \frac{2\mu_g}{\alpha_g}\left(\lambda^{\alpha_g - 1} - \lambda^{\frac{\alpha_g}{2} - 1}\right) + \frac{2\mu_a}{\alpha_a}\left(\lambda^{\alpha_a - 1} - \lambda^{\frac{\alpha_a}{2} - 1}\right) . \tag{25}$$

Recent tests using the isotropic first order Ogden formulation ($\mu_a = 0$ in Eq. 25) show that the shear modulus of the material can change along different shear testing directions, but the nonlinear behavior of the material (α) is not sensitive to the test direction. From these observations, the stress–stretch relationship is adjusted accordingly ($\alpha_a = \alpha_g = \alpha$).

2.2
Structural model formulations

In a traction-free state, the axonal segments within the optic nerve appear compressed, or undulated to varying degrees (Bain et al. 1996; Fig. 1). Due to the initial undulated appearance of axons in the optic

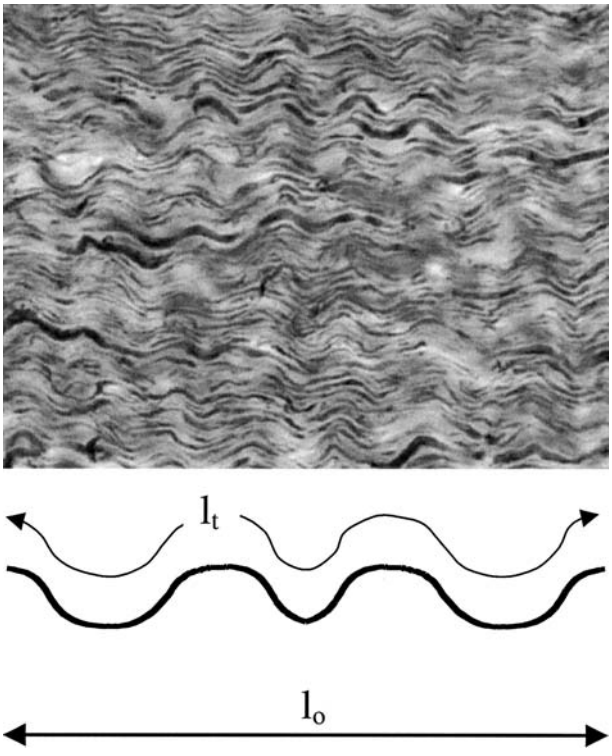

Fig. 1. Microstructural geometry of myelinated CNS axons within a white matter tract, the guinea pig optic nerve. Axons are visualized using neurofilament immunohistochemistry, and appear "wavy" or undulated under in situ length conditions. Undulation (U), defined as the ratio of the true axonal length (l_t) to the end-to-end distance (l_o), is used to characterize the microstructural appearance of the axons at a point in the white matter

nerve, only a portion of the axonal population will experience tensile strains during elongation. To estimate the strain experienced by an axon within an elongated nerve, structurally based models of the optic nerve can be developed along similar lines to the structural models formulated for other soft tissues (see, for example, Frisen et al. 1969; Haut and Little 1972; Comninou and Yannas 1976; Lanir 1979; Kastelic et al. 1980; Decraemer et al. 1980; Shoemaker et al. 1986; Kwan and Woo 1989; Belkoff and Haut 1991; Cohen et al. 1992; Spilker et al. 1992; Woo et al. 1993; Zhu et al. 1994; Skaggs et al. 1994).

We will define the undulation of an axon within the tissue by an undulation parameter (U):

$$U = \frac{l_t}{l_o} \quad , \tag{26}$$

where l_o is the distance between two points at the beginning and end of the axon section (Fig. 1), while l_t is the "true" length of the axon if it were straightened to eliminate the undulations. Note that l_o is an updated/current length, hence U does not contain deformation information. For U values greater than 1.0, the axon is undulated in the tissue and bears no tensile force. In contrast, $U = 1.0$ indicates that the axon is completely straight and can support a tensile force.

All axons in a longitudinal section of the optic nerve tissue will not show the same undulated appearance (Fig. 1). For this reason, three simple population distribution functions will be used to describe the variation in the undulation parameter (U):

1. The axonal population shows a uniform distribution between two values of undulation – U_{min} and U_{max}. The population density function for axons at a given undulation value (U) is α, where

$$f(U) = \alpha = \frac{1}{U_{max} - U_{min}} \quad , \tag{27}$$

   given that $U_{min} < U < U_{max}$. The probability density function is zero elsewhere.
2. The axonal undulation parameter shows a normal statistical distribution, similar to the assumptions for collagen fiber in connective tissue (Decraemer et al. 1980), and therefore has the probability density function ($f(U)$):

$$f(U) = \frac{1}{\sqrt{2\pi\sigma}} \exp\left(\frac{-(U-\mu)^2}{2s^2}\right) \quad . \tag{28}$$

   A mean undulation factor (μ) and standard deviation (σ) for distribution can be developed by using measurements from histologic sections.

3. The axonal undulation parameter is measured directly from histological sections, and the experimental probability density function, $f(U_i)$, is developed at discrete points over the undulation interval $U_{\min} < U_i < U_{\max}$. In this description, the subscript i denotes a specific value of the undulation parameter over the measured range.

By elongating a section of optic nerve tissue by an amount δ, the axons in each of these three populations described above begin to straighten and the undulation distribution changes in proportion to the applied displacement. An axon (undulation, U) stretches when the tissue stretch ratio (λ) is greater than the undulation value. The axon stretch ratio (λ_a) is given by:

$$\lambda_a = \frac{\lambda}{U} \quad . \tag{29}$$

The axial force generated by the axon during elongation is given by the product of the engineering stress, (T_{axon}) say, and the undeformed axon area (A_{axon}):

$$F_{axon} = T_{axon} A_{axon} \quad . \tag{30}$$

The exact constitutive relationship for a single axon in the optic nerve is not known. Therefore, it is assumed that (T_{axon}) for an axon stretched a known amount (λ_a) follows a simple neo-Hookean relationship:

$$T_{axon} = C\left(\lambda_a - \frac{1}{\lambda_a^2}\right) \quad , \tag{31}$$

which applies for $\lambda_a > 1.0$. In (31) C denotes a stress-like material parameter. The total force from the axons in the white matter is a summation of the forces generated within each axon:

$$F_{axons,total} = \int_{U=1}^{U=U_{max}} N \cdot A_{axon} \cdot f(U) \cdot C\left(\frac{\lambda}{U} - \frac{U^2}{\lambda^2}\right) dU \quad , \tag{32}$$

where $f(U)$ is a probability distribution function for the axonal undulation of the population and N is the number of axons in the tissue. For simplification, it is assumed that the axons in the population are spread across a narrow diameter range, and therefore the axon cross-sectional area is considered approximately constant across the population.

Previous work has shown that the matrix surrounding myelinated axons in CNS tissue – i.e., the supporting glial cells and the capillary network – has an approximately three-fold lower complex compliance at low strain values (Arbogast and Margulies 1999). Additionally, the surrounding matrix represents approximately 10% of the total volume of tissue in the optic nerve. Assuming the glia is represented as a neo-Hookean material ($C_{glia} = 0.33\ C_{axon} = 3C$) and is 10% of the cross-sectional area, the force generated in the glia during simple extension is:

$$F_{glia} = 0.33C\left(\lambda - \frac{1}{\lambda^2}\right)(0.1\ A_{nerve}) = 0.033C\left(\lambda - \frac{1}{\lambda^2}\right)A_{nerve} \quad . \tag{33}$$

As a result, the total force in the optic nerve is a summation of the forces from the individual axons and the glia:

$$\begin{aligned} T_{nerve} &= \frac{F_{glia} + F_{axons,total}}{A_{nerve}} \\ &= \frac{0.033 A_{nerve} C\left(\frac{\lambda}{U} - \frac{U^2}{\lambda^2}\right) + N \cdot A_{axon} \cdot \int_{U=1}^{U=U_{max}} f(U) \cdot C\left(\frac{\lambda}{U} - \frac{U^2}{\lambda^2}\right) dU}{A_{nerve}} \quad . \end{aligned} \tag{34}$$

Since the axons represent 90% of the cross-sectional area in the optic nerve, the engineering stress relationship simplifies to:

$$T_{nerve} = 0.033C\left(\frac{\lambda}{U} - \frac{U^2}{\lambda^2}\right) + 0.9 \int_{U=1}^{U=U_{max}} f(U) \cdot C\left(\frac{\lambda}{U} - \frac{U^2}{\lambda^2}\right) dU \quad . \tag{35}$$

The computed stress in the nerve at a specific applied stretch ratio (λ) will assume three general forms based on the three distinct distributions assumed for the axons appearing within the nerve:

1. The axons display a uniform undulation distribution between $U_{\min}$ and $U_{\max}$. Since there may be values of tissue stretch where not all axons are elongated, this stress–stretch relationship assumes three forms:
   For $\lambda < U_{\min}$:

$$T(\lambda) = 0.033C\left(\frac{\lambda}{U} - \frac{U^2}{\lambda^2}\right) \ , \tag{36}$$

   For $U_{\min} < \lambda < U_{\max}$:

$$T(\lambda) = 0.033C\left(\frac{\lambda}{U} - \frac{U^2}{\lambda^2}\right) + 0.9\int_{U=1}^{U=\lambda} \alpha \cdot C\left(\frac{\lambda}{U} - \frac{U^2}{\lambda^2}\right)\mathrm{d}U \ , \tag{37}$$

   or, equivalently,

$$T(\lambda) = 0.033C\left(\frac{\lambda}{U} - \frac{U^2}{\lambda^2}\right) + \alpha C\left[\lambda \ln\left[\frac{\lambda}{U_{\min}}\right] - \frac{1}{3}\frac{\left(\lambda^3 - U_{\min}^3\right)}{\lambda^2}\right] \ . \tag{38}$$

   For $\lambda > U_{\max}$:

$$T(\lambda) = 0.033C\left(\frac{\lambda}{U} - \frac{U^2}{\lambda^2}\right) + \alpha C\left[\lambda \ln\left(\frac{U_{\max}}{U_{\min}}\right) - \frac{1}{3}\frac{\left(U_{\max}^3 - U_{\min}^3\right)}{\lambda^2}\right] \ . \tag{39}$$

2. The undulation of the axons follows a normal distribution. In this case, an integral expression describing the resulting stress–stretch relationship is obtained:

$$T(\lambda) = 0.033C\left(\frac{\lambda}{U} - \frac{U^2}{\lambda^2}\right) + \int_{U=1}^{U=\lambda} f(U) \cdot C\left(\frac{\lambda}{U} - \frac{U^2}{\lambda^2}\right)\mathrm{d}U \ , \tag{40}$$

   which is computed numerically over the interval.
3. The undulation of the axons follows a distribution measured experimentally in a series of longitudinally sectioned axons (Bain and Meaney 2000). Assuming the probability distribution function ($f_i(U_i)$) is described over M subintervals, the stress–stretch behavior is calculated directly:

$$T(\lambda) = 0.033C\left(\frac{\lambda}{U} - \frac{U^2}{\lambda^2}\right) + \sum_{i=1}^{M} f_i(U_i) \cdot \Delta U_i \cdot C\left(\frac{\lambda}{U_i} - \frac{U_i^2}{\lambda^2}\right) \ . \tag{41}$$

2.3
Comparison of continuum models with structural models

With continuum and structural representations now developed for the uniaxial testing configuration, attention is placed on the similarities and differences between these two classes of models. Comparisons are made to determine the equivalence between the continuum models and the structural models, and to quantify the differences that occur when a continuum approach is used.

To draw parallels between the continuum and structural models, constants for the hyperelastic material descriptions are computed using a least squares minimization procedure (IgorPro, Wavemetrics, Inc.) that best fit the recruitment phenomena appearing in the structural model. Constants are constrained to ensure positive definiteness for the strain–energy function under tensile, compressive, and shear loading conditions. For the structural models, parameters describing the axonal undulation were selected to provide representations of undulations measured in histologic sections (average undulation = 1.131, standard deviation = 0.0633). For the uniform representation, a minimum undulation of 1.0 was used, with a maximum undulation of 1.262.

Since it is likely that the continuum and structural models will not match exactly, we introduce a normalized error term that describes the relative difference between the two approximations at an applied stretch level (λ):

$$e_r = \frac{|\sigma_c(\lambda) - \sigma_s(\lambda)|}{\sigma_s(\lambda)} \tag{42}$$

where c denotes the continuum (hyperelastic) formulation, s indicates the structural model formulation and e_r is the error residual. From the best fits, we determine the residual terms across the range of stretch levels below and above the threshold associated with axonal injury caused by simple extension ($\lambda < 1.5$).

3 Model results

With these formulas as background, the methods are applied to a realistic representation of a highly oriented white matter tract, the guinea pig optic nerve. Previous work has shown that the axons are undulated in this white matter tissue (Bain et al. 1996), and that measured undulation is approximated as a gamma distribution. Modeling this exact statistical distribution is beyond the scope of this paper; rather, we will either approximate or use these recent measurements of axonal geometry in each of our structural models to draw comparisons with "equivalent" hyperelastic models.

Typically, an average undulation for the entire population of axons within the optic nerve is $U_a = 1.13$. Using this as the midpoint in a uniform distribution ($U_{min} = 1.0$; $U_{max} = 1.26$), Fig. 2a shows the resulting structural model response, along with the "equivalent" Mooney–Rivlin, Fung, and generalized Ogden formulation. With this structural model formulation, a gradual change in stress occurs as an increasing fraction of the axons are elongated. Once all axons are "recruited" into tensile loading ($\lambda > 1.26$), the structural models show a slightly softening behavior in the "straightened" phase. Table 1 shows the hyperelastic constants associated with the structural model predictions, indicating the Mooney–Rivlin model is the least precise of the continuum approximations, while the remaining continuum models offer a substantial improvement to this formulation. Both the first order Ogden material and the Fung formulation are sufficiently flexible to model the nonlinear stress–stretch relationship predicted for the optic nerve.

Using the second structural modeling approach where the axon undulation shows a normal distribution, estimates of the distribution parameters ($\mu_u = 1.13$, $\sigma_u = 0.063$) are used from measurements on longitudinal sections of the optic nerve. Figure 2b contains the predicted response from this structural model, as well as the equivalent hyperelastic models. Much like the first structural model, there is a nonlinear phase where the number of recruited axons increases with applied stretch to produce a nonlinear engineering stress–stretch relationship, followed by a more linear phase. With the increasing complexity of the structural model, the correlation to the equivalent material model improves over other approaches (Table 1).

For the third structural modeling approach, direct measurement of the axonal geometry in the resting in situ state was utilized to predict the resulting engineering stress–stretch relationship (Fig. 2c). The nonlinear response observed over the entire range reflects the increasing fraction of axons stretched as the applied tensile deformation increases. Similar to previous structural models, the generalized Ogden and Fung material approximations are more reasonable estimates of the predicted structural response (Table 1) than the isotropic Mooney–Rivlin formulation.

Across the three structural models, the recruitment of axons during the early phase of stretching accounted for the most significant difference among the three model formulations (Fig. 3). For the uniform distribution, the stress built up quickly as a linearly increasing fraction of axons were elongated at the lowest stretch levels. In contrast, the approximate normal and measured statistical distributions of axonal geometry indicated only a small fraction of the axons were experiencing tensile loads, and therefore the resulting force at lower elongation levels ($\lambda < 1.2$) was significantly different than the uniform distribution condition. Interestingly, the difference in engineering stress–stretch responses using the approximate normal distribution and the actual measured axonal geometry varied by less that 5% across the entire range. The close agreement between the approximated normal distribution and measured microstructure population suggests that the axonal population can be approximated as normally distributed without significant loss in precision, an assumption that has been used by investigators examining other soft tissues (Lanir 1979).

Of the three continuum approximations, the Mooney–Rivlin was the poorest approximation to the stress–stretch predictions from all structural model formulations, showing a significant error term at all elongation levels (Fig. 4a). The Mooney–Rivlin formulation was not capable of modeling both the recruitment of axons during the early phase of elongation, nor the relatively straight stress–stretch relationship that occurred once the complete axonal population supported tensile loading. Indeed, adjusting both the shear constant and the nonlinear behavior with

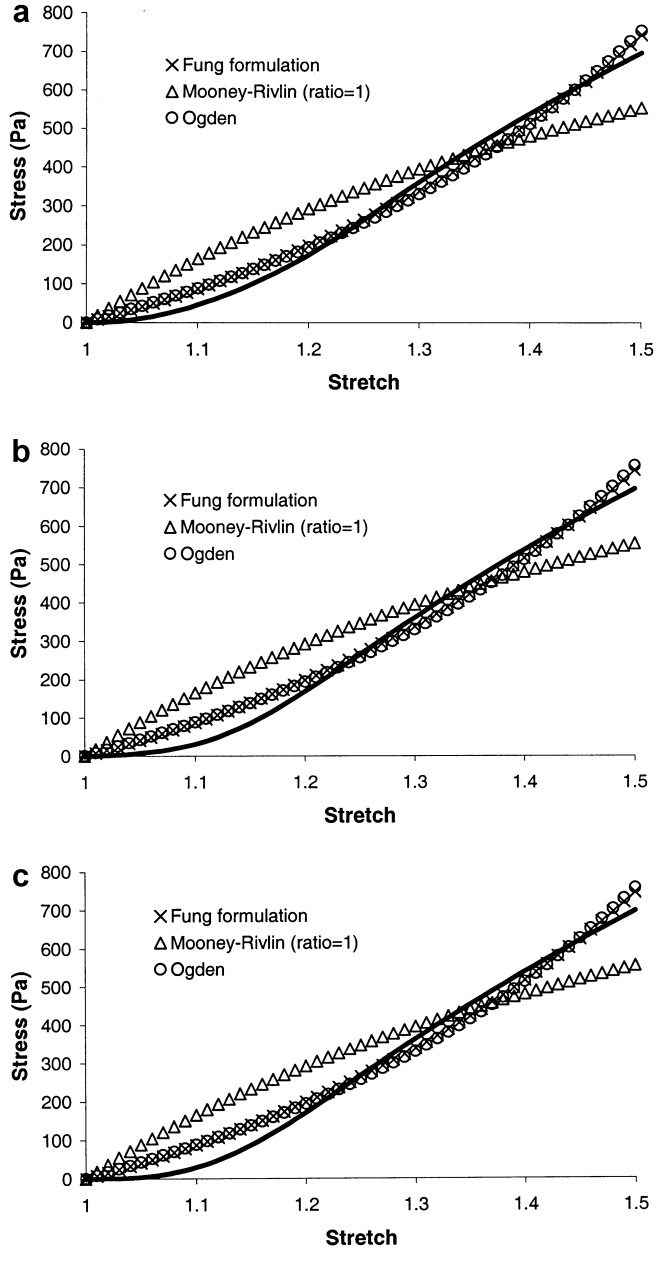

Fig. 2a–c. Comparison of structurally based models (*solid line*) with continuum models (*symbols*) based on hyperelastic descriptions. Assuming distinct frequency distributions (**a** uniform frequency; **b** normal distribution; c measured empirical distribution) for the axonal microstructure (U), the nonlinear engineering stress–stretch relationship is consistently best modeled using either a first order Ogden strain–energy function or the exponential strain–energy function proposed by Fung

stretch were necessary to provide a reasonable continuum approximation to the results from the structural models, as shown by the approximation of the Fung and first order Ogden materials (Fig. 4b, c). Normalized errors with both anisotropic formulations were substantially less than the Mooney–Rivlin approximations, and the errors were minimized across the entire elongation range.

Each structural model showed an initial increase in the slope of the stress–stretch curve, described as the tangential stiffness, until all axons began to assume some level of tensile stress (Fig. 5a). The tangential stiffness range was similar across the three structural formulations, but was not matched well by the computed tangential stiffness characteristics for the continuum models (Fig. 5b). Simple continuum models (neo-Hookean, Mooney–Rivlin) showed a decreasing stiffness over the entire stretch range, while the generalized first order Ogden and Fung materials displayed an increasing stiffness across the elongation interval. Additionally, tangential stiffness was not sensitive to the ratio of Mooney–Rivlin shear constants used in the continuum approximations. The disparity between the tangential stiffness characteristics of continuum approximations and the structurally based models was consistent across the three structural models, with little differences noted across the elongation range studied.

Table 1. Comparison of structural models and continuum approximations

Population description for axonal microstructure	Continuum model approximation (Constants (Pa), average error residual e_r^{ave})		
	Mooney–Rivlin	Fung formulation	Generalized Ogden
Uniform			
f(U)=α	μ_1/μ_2=10, μ_1=514.36 (Pa), e_r^{ave}=3.54	C=1,573.61 (Pa),	μ=290.82 (Pa), α=6.19
For $U_1<U<U_2$	μ_1/μ_2=1, μ_1=315.7 (Pa), e_r^{ave}=3.93	$C_2=10\mu_2$	e_r^{ave}=1.722
f(U)=0 elsewhere	μ_1/μ_2=0.1, μ_2=647.6 (Pa), e_r^{ave}=4.42	$\mu_2=5.61\times10^{-3}$	
		e_r^{ave}=1.53	
Normal			
$f(U)=\frac{1}{\sqrt{2\pi\sigma}}e^{-(U-\mu)^2/2\sigma^2}$	μ_1/μ_2=10, μ_1=510.19 (Pa), e_r^{ave}=2.71	C=1,200.1 (Pa),	μ=279.27 (Pa), α=6.36
	μ_1/μ_2=1, μ_1=313.02 (Pa), e_r^{ave}=3.00	$C_2=10\mu_2$	e_r^{ave}=1.28
	μ_1/μ_2=0.1, μ_2=641.8 (Pa), e_r^{ave}=3.36	$\mu_2=7.19\times10^{-3}$	
		e_r^{ave}=1.17	
Measured			
	μ_1/μ_2=10, μ_1=511.52 (Pa), e_r^{ave}=5.84	C=1,255.5 (Pa),	μ=281.84 (Pa), α=6.33
	μ_1/μ_2=1, μ_1=313.84 (Pa), e_r^{ave}=6.46	$C_2=10\mu_2$	e_r^{ave}=1.28
	μ_1/μ_2=0.1, μ_2=643.5 (Pa), e_r^{ave}=7.22	$\mu_2=5.61\times10^{-3}$	
		e_r^{ave}=2.64	

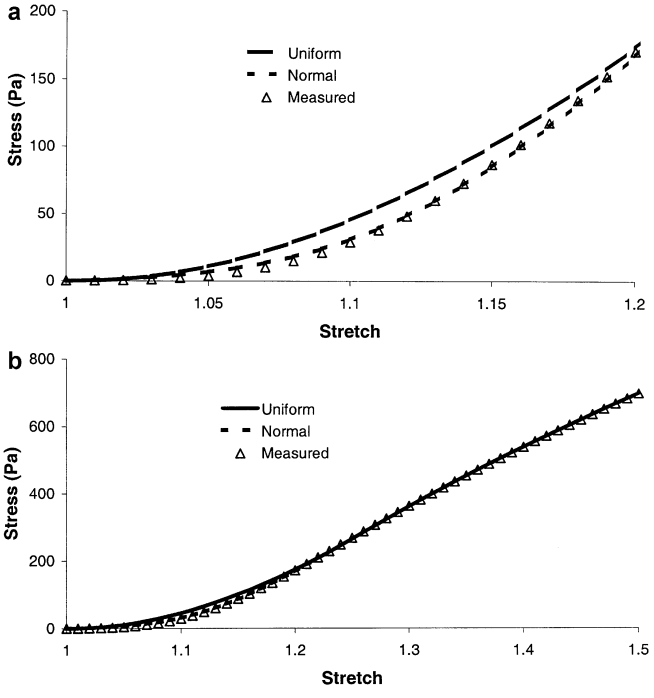

Fig. 3a, b. Relative comparison of the three structural model formulations. **a** At lower elongation levels, differences among the three structural models appeared, with the uniform distribution model showing the most rapid increase in the stress generated within the optic nerve. **b** At higher elongation regions, relatively small differences appeared among the three formulations, each reaching similar peak stress levels at the highest elongation levels

4 Discussion

In this paper, relationships between simple structural models of a white matter tract were compared with equivalent continuum approximations using hyperelastic material formulations. Both isotropic and anisotropic hyperelastic formulations were developed, with reinforcing axonal fibers producing a

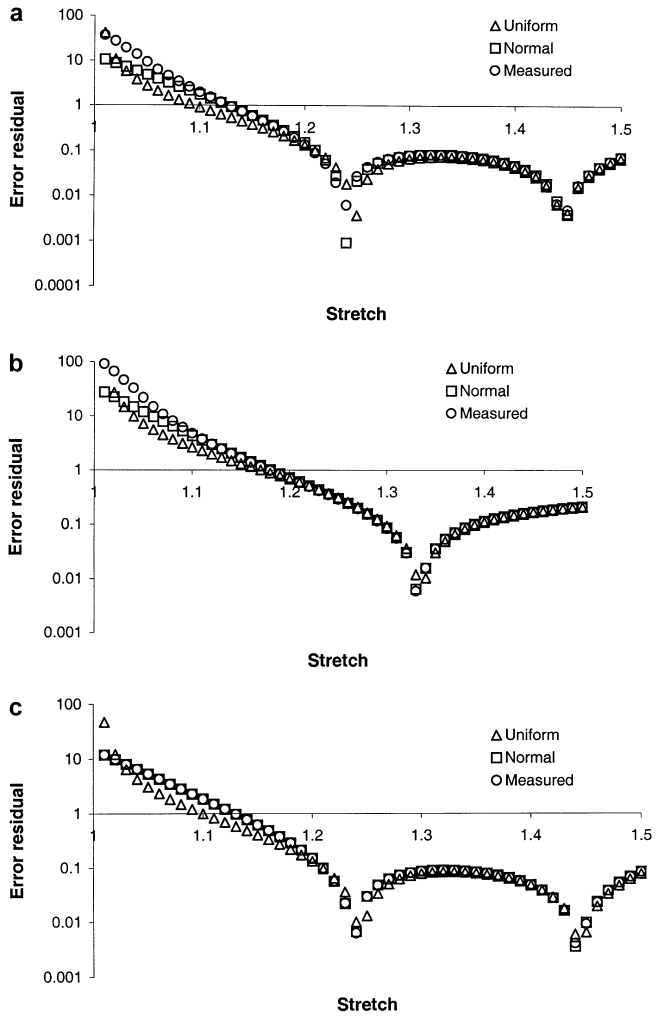

Fig. 4a–c. Error residual comparison between continuum approaches and structural model descriptions of white matter behavior. The Mooney–Rivlin formulation (**a**) showed the least consistent match with structural model predictions (noted as *symbols*) over the range examined. The Fung (**b**) and first order Ogden (**c**) formulations showed the closest agreement to the structural models

transversely isotropic hyperelastic material. All three structurally based models of the CNS white matter under simple extension loading showed similar stress–stretch characteristics at larger elongation levels ($\lambda > 1.2$). Moreover, each structurally based model showed an initial phase of rapidly increasing tangential stiffness, followed by a phase of decreasing stiffness at higher elongation levels. Only a more generalized hyperelastic model used in this study – a first order Ogden model and Fung formulation – was capable of providing a reasonable approximation of the structural model responses over the elongation range studied ($\lambda < 1.5$). However, neither the generalized form of the Ogden formulation nor the Fung formulation could model the complete tangential stiffness behavior predicted by the three structural modeling approaches.

Recent studies of the material properties of brain tissue have used isotropic hyperelastic material descriptions to model the measured response of the CNS tissue to shear, compression, or combined loading, reflecting an increasing interest in moving from phenomenological approaches to material formulations that are readily available in commercial finite element packages. Mendis et al. (1995) were the first to apply a hyperelastic energy based approach to model the constitutive behavior of brain tissue under compression (Galford and McElhaney 1970), yielding a reasonable approximation of the response under compression and showing the sensitivity of the compression response to the two material constants in the Mooney–Rivlin formulation. However, the same formulation was not successful in modeling the response of white and mixed gray/white matter samples to shear deformation (Prange et al. 2000). Rather, a generalized first order Ogden material proved more capable of modeling the tissue response under shear and compression (Prange et al. 2000). When combined with a time dependent description of the material shear modulus, the Ogden characterization could be extended to accurately model the response of tissue under both dynamic shear and compression conditions.

Although there is recent information describing the response of brain tissue under finite strains, only recently has the material anisotropy of brain tissue been clarified. In a series of shear testing

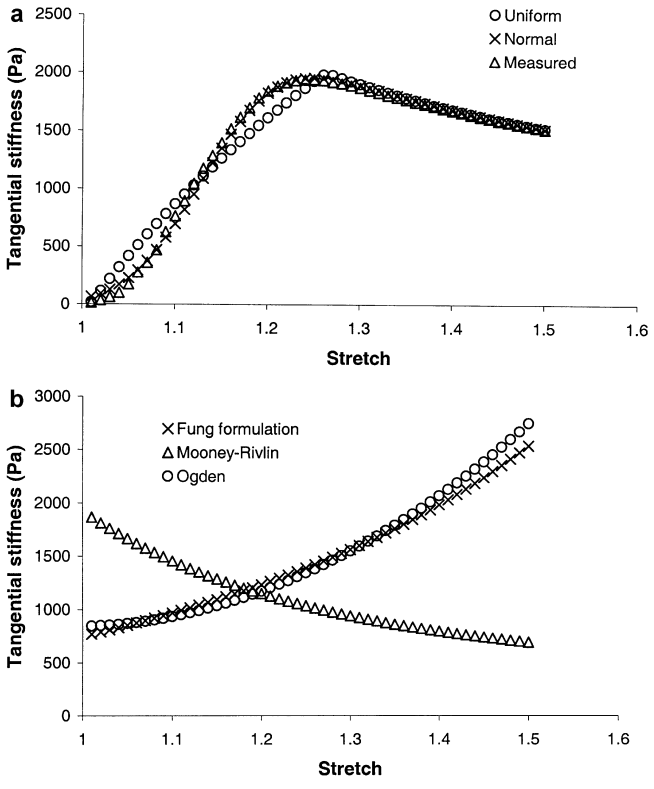

Fig. 5a, b. Comparing the tangential stiffness behavior for structural models (panel **a**) and continuum approximations of the white matter (panel **b**). **a** Similar tangential stiffness values appeared over the entire range of stretch for the structural models. **b** Only the generalized Ogden and Fung formulations (*symbols*) were capable of modeling the initial increase in tangential stiffness observed in **a**. At higher elongation levels, the Mooney–Rivlin was the only continuum approximation to show a decline in stiffness similar to the decrease observed in the structural models

experiments using gray matter, mixed gray matter/white matter, oriented white matter (corpus callosum), and randomly oriented white matter (corona radiata) samples, Prange and Margulies (2002) reported that highly oriented tissue samples could exhibit shear properties that varied significantly with testing direction. For the highly aligned corpus callosum samples, the shear moduli in a direction along the fiber direction was nearly double the shear modulus measured transverse to the fiber direction. For other less aligned white matter samples, as well as all gray matter samples, no effect of testing direction was observed. These experimental data emphasize the importance of developing hyperelastic formulations that account for preferred fiber orientations, and the two anisotropic formulations in this paper attempt to examine how a structural representation of the white matter translates into hyperelastic formulations that are capable of modeling anisotropic behavior. The formulations in this study were restricted to transverse isotropy caused by a single population of axonal fibers aligned uniformly along one direction. Extending these formulations to include a more heterogeneous population of directional fibers is possible, and could be useful to understand the directional properties of less organized regions of the white matter such as the corona radiata. Moreover, the utility of the relative simple Ogden and Fung material formulations in describing a structurally based material response, in addition to the previous use of the Ogden formulation to model measured brain material properties, points to an opportunity for further using the simple anisotropic characterization to relate continuum properties to, ultimately, estimates of the cellular response that occurs within the white matter tissue.

Although there was a reasonable match between the stress–stretch relationships developed from the generalized Ogden and Fung formulations and all three structural models, there was less agreement among the approaches when examining the tangential stiffness response of the models across the loading regime. Differences in the tangential stiffness between the two approaches may lead to significant differences in stress predictions over more complex loading profiles, and therefore should be minimized if possible. In the current study, the tangential stiffness of the structural models uniformly decreased beyond the transition point where no additional axons were "recruited" into the stress–stretch relationship ($\lambda \sim 1.26$). However, the decreasing tangential stiffness noted in the structural models is linked directly to the underlying constitutive relationship assigned to individual axons within the white matter tract. Only an approximation of the single axonal constitutive relationship was used in this study, and therefore an accurate measure of the tangential stiffness of the structural model remains to be determined. For example, a preliminary examination of structural models using stress–stretch relationships derived from the myelinated

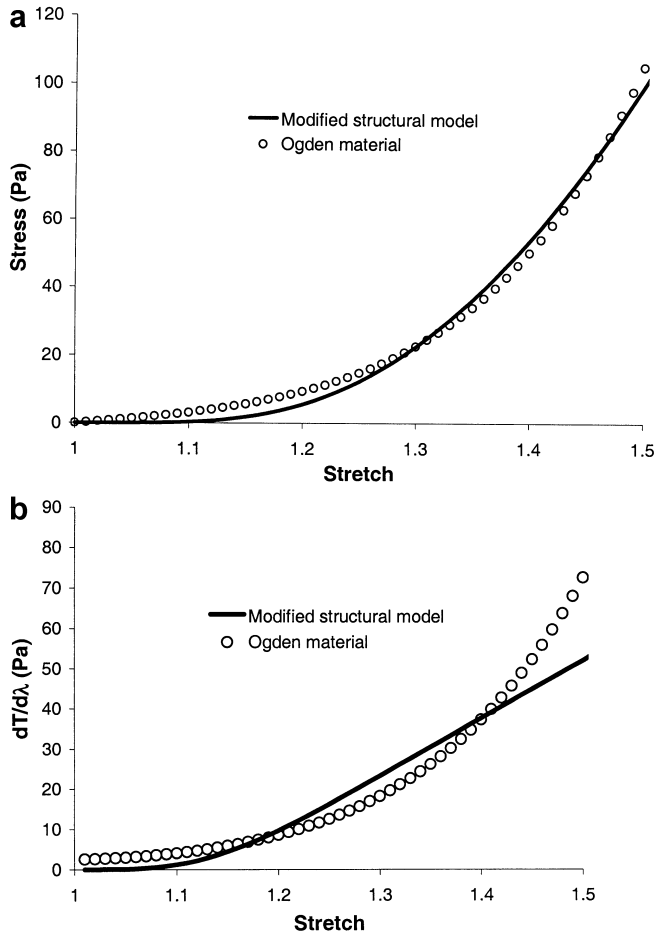

Fig. 6a, b. Influence of axonal constitutive relationship on tangential stiffness. **a** By replacing the axonal constitutive relationship with an expression measured for single, myelinated PNS axons ($\sigma=C(\lambda-1)^2$), the tangential stiffness behavior for the structural model changed to reflect an increasing stiffness across the entire elongation range (*solid line*), a trend that was matched with an appropriately fit generalized Ogden formulation (*dashed line*). **b** General agreement for the engineering stress–stretch response was obtained between this revised structural model and the first order Ogden model

peripheral nerve fiber ($\sigma_{\text{fiber}} = C(\lambda-1)^2$; Saatman and Thibault, 1993) show that the tangential stiffness increases over the entire regime with this new relationship, with little effect on the ability of the generalized Ogden formulation to fit the response over the entire loading range (Fig. 6). Significant structural differences exist between peripheral nerve fibers and myelinated CNS axons – the cytoskeletons are distinct, the myelinating cell types are different, and the node of Ranvier is protected in the peripheral nervous system (PNS) nerve fiber with a surrounding matrix while the node is exposed in the CNS (Waxman et al. 1995) – and therefore precludes using this fiber constitutive relationship directly in the current study. However, as more specific information on individual CNS axonal properties becomes available, the comparisons of the tangential stiffness between continuum and structurally based modeling approaches will become increasingly meaningful and predictive of the ability to match a structural model response over more complex loading regimes.

The underlying finding of the structurally based models of the white matter used in this report – i.e., increasing the applied tissue elongation results in an increasing fraction of individual axons "sensing" tensile loading – suggests that the resulting pathophysiological response of axons within the tissue experiencing a specific stretch would not be uniform. Indeed, the spectrum of axonal stress levels that occur at a specific elongation level provides a potential explanation for the scattered appearance of injured axonal fibers among a much larger population of uninjured axons in the white matter tract. At higher levels of applied strain, the relative fraction of injured to uninjured axons increases proportionally (Bain et al. 1996), again consistent with the prediction that more axons will experience a tensile load above a pathophysiological limit. However, the mechanical recruitment phenomena should not be considered the sole factor responsible for this nonlinear injury response. Recent in vitro studies using cultured axons shows that exposing unmyelinated axons to the same level of applied stretch does not result in a uniform pathophysiological response – some axons display significant ionic shifts, while others in the same population show very little overt change from baseline values and little long term morphological changes (Wolf et al. 2000). Thus, it appears that axonal populations also need to be modeled more explicitly to account for potentially different mechanical

and biological characteristics, both of which dictate the injury response relationship observed in white matter tissue.

In closing, comparing hyperelastic models and structurally based models will be important to consider when predicting the circumstances that cause axonal injury in the white matter in humans. By comparing the structural model with an appropriate continuum model, fairly powerful finite element models can be used quickly to predict better the motions and tissue movements that are associated with injury. Perhaps more importantly, we will be positioned to solve the "hierarchical problem" – estimating deformations of cellular and subcellular structures from the deformations predicted using continuum material models. Together, these parallel efforts will allow us to use computationally less expensive continuum formulations to model more accurately the structural response of the brain during impact, yet retain a relationship to the underlying structural elements that will form the basis for the next generation of models to predict the biological response of the tissue to applied mechanical loading.

References

Arbogast, K.B.; Margulies, S.S.: A fiber-reinforced composite model of the viscoelastic behavior of the brainstem in shear. J Biomech 32 (1999) 865–870

Bain, A.C.; Meaney, D.F.: Tissue level thresholds for axonal damage in an experimental model of central nervous system white matter injury. J Biomech Eng 122 (2000) 615–622

Bain, A.C.; Billiar, K.L.; Shreiber, D.I.; McIntosh, T.K.; Meaney, D.F.: In vivo mechanical thresholds for traumatic axonal damage. AGARD Specialists Meeting, Mescalero, New Mexico. North Atlantic Treaty Organization (NATO), Washington, DC (1996)

Belkoff, S.M.; Haut, R.C.: A structural model used to evaluate the changing microstructure of maturing rat skin. J Biomech 24 (1991) 0711–720

Cohen, B.; Chorney, G.S.; Phillips, D.P.; Dick, H.M.; Buckwalter, J.A.; Ratcliffe, A.; Mow, V.C.: The microstructural tensile properties and biochemical composition of the bovine distal femoral growth plate. J Orthop Res 10 (1992) 263–275

Comninou, M.; Yannas, I.V.: Dependence of stress–strain nonlinearity of connective tissues on the geometry of collagen fibers. J Biomech 9 (1976) 427–433

Decraemer, W.F.; Maes, M.A.; Vanhuyse, V.J.; Vanpeperstraete, P.: A non-linear viscoelastic constitutive equation for soft biological tissues, based upon a structural model. J Biomech 13 (1980) 559–564

Frisen, M.; Magi, M.; Sonnerup, L.; Viidik, A.: Rheological analysis of soft collagenous tissue, Part I: Theoretical considerations. J Biomech 2 (1969) 13–20

Fung, Y.C.: Mechanical properties of living tissues. Springer-Verlag, New York Berlin Heidelberg (1981)

Galbraith, J.; Thibault.; L.E.; Matteson, R.: Mechanical and electrical responses of the squid axon to simple elongation. J Biomech Eng 115 (1993) 13–22

Galford, R.; McElhaney, J.: A viscoelastic study of scalp, brain, and dura. J Biomech 3 (1970) 211–221

Gennarelli, T.A.; Thibault, L.E.; Tipperman, R.; Tomei, G.; et al.: Axonal injury in the optic nerve: a model simulating diffuse axonal injury in the brain. J Neurosurg 71 (1989) 244–253

Gray, J.A.B.; Ritchie, J.M.: Effects of stretch on single myelinated nerve fibers. J Physiol 124 (1954) 84–99

Haut, R.C.; Little, R.W.: A constitutive equation for collagen fibers. J Biomech 5 (1972) 423–430

Kastelic, J.; Palley, I.; Baer, E.: A structural mechanical model for tendon crimping. J Biomech 13 (1980) 887–893

Kwan, M.; Woo, S.L.: A structural model to describe the nonlinear stress–strain behavior for parallel fibered collagenous tissues. J Biomech Eng 111 (1989) 361–363

Lanir, Y.: A structural theory for the homogenous biaxial stress–strain relationships in flat collagenous tissues. J Biomech 12 (1979) 423–436

Mendis, K.K.; Stalnaker, R.L.; Advani, S.H.: A constitutive relationship for large deformation finite element modeling of brain tissue. J Biomech Eng 117 (1995) 279–285

Morrison, B.; Saatman, K.E.; Meaney, D.F.; McIntosh, T.K.: In vitro central nervous system models of mechanically induced trauma: a review. J Neurotrauma 15 (1998) 220–234

Ogden, R.W.: Non-linear elastic deformations. Dover, Mineola, N.Y. (1984)

Prange, M.; Meaney, D.; Margulies, S.: Defining brain material properties: effect of region, direction, and species. Stapp Car Crash J 44 (2000) 205–213

Prange, M.; Margulies, S.: Regional, directional, and age-dependent properties of the brain undergoing large deformation. J Biomech Eng 124 (2002) 244–252

Rydevik, B.L.; Kwan, M.K.; Myers, R.R.; Brown, R.A.; Triggs, K.J.; Woo, SL.; Garfin, S.R.: An in vitro mechanical and histological study of acute stretching on rabbit tibial nerve. J Orthop Res 8 (1990) 694–701

Saatman, K.E.; Thibault, L.E.: Response of the single myelinated nerve fiber to dynamic stretch. In: Proceedings of the International Research Council on the Biomechanics of Impact (IRCOBI) Conference, Berlin, Germany, pp. 216–223 (1993)

Shoemaker, P.A.; Schneider, D.; Lee, M.D.; Fung, Y.C.: A constitutive model for two-dimensional soft tissues and its application to experimental data. J Biomech 19 (1986) 695–702

Skaggs, D.L.; Weidenbaum, M.; Iatridis, J.D.; Ratcliffe, A.; Mow, V.C.: Regional variation in tensile properties and biochemical composition of the human lumbar annulus fibrosis. Spine 19 (1994) 1310–1319

Spencer, A.J.M.: Continuum theory of the mechanics of fiber reinforced composites. Springer-Verlag, New York Berlin Heidelberg (1984)

Spilker, R.L.; Donzelli, P.S.; Mow, V.C.: A transversely isotropic biphasic finite element model of the meniscus. J Biomech 25 (1992) 1027–1045

Wall, E.J.; Kwan, M.D.; Rydevik, B.L.; Woo, S.L.; Garfin, S.R.: Stress relaxation of a peripheral nerve. J Hand Surg [Am] 16 (1991) 859–863

Waxman, S.G. (ed.): The axon: structure, function, and pathophysiology. Oxford University Press, New York (1995)

Wolf, J.A.; Stys, P.A.; Lusardi, T.; Meaney, D.; Smith, D.: Traumatic axonal injury induces calcium influx modulated by tetrodotoxin-sensitive sodium channels. J Neurosci 21 (2000) 1923–1930

Woo, S.L.; Johnson, G.A.; Smith, B.A.: Mathematical modeling of ligaments and tendons. J Biomech Eng B 115 (1993) 468–473

Zhu, W.; Chern, K.Y.; Mow, V.C.: Anisotropic viscoelastic shear properties of bovine meniscus. Clin Orthop 306 (1994) 34–45